Cloud Impacts on Pavement Temperature and Shortwave Radiation

CURTIS L. WALKER AND MARK R. ANDERSON

Department of Earth and Atmospheric Sciences, University of Nebraska–Lincoln, Lincoln, Nebraska

(Manuscript received 26 February 2016, in final form 9 August 2016)

ABSTRACT

Forecast systems provide decision support for end users ranging from the solar energy industry to municipalities concerned with road safety. Pavement temperature is an important variable when considering vehicle response to various weather conditions. A complex relationship exists between tire and pavement temperatures that affects vehicle performance. Many forecast systems suffer from inaccurate radiation forecasts resulting in part from the inability to model different types of clouds and their influence on radiation. This research focuses on forecast improvement by determining how cloud type impacts pavement temperature and the amount of shortwave radiation reaching the surface. The study region is the Great Plains where surface radiation data were obtained from the High Plains Regional Climate Center's Automated Weather Data Network stations. Pavement temperature data were obtained from the Meteorological Assimilation Data Ingest System. Cloud-type identification was possible via the Naval Research Laboratory Cloud Classification algorithm, and clouds were subsequently sorted into five distinct groups: clear conditions, low clouds, middle clouds, high clouds, and cumuliform clouds. Statistical analyses during the daytime in June 2011 revealed that cloud cover lowered pavement temperatures by up to approximately 10°C and dampened downwelling shortwave radiation by up to 400 W m^{-2}. These pavement temperatures and surface radiation observations were strongly correlated, with a maximum correlation coefficient of 0.83. A comparison between cloud-type group identified and cloud cover observed from satellite images provided a measure of confidence in the results and identified cautions with using satellite-based cloud detection.

1. Introduction

Pavement temperature forecasts provide critical information to local officials, transportation industry interests, and the general public, whether traveling for business or pleasure, and are imperative in the prevention of loss of life and damage to property (Pisano et al. 2008; Chen et al. 2009; Khasawneh and Liang 2012; Federal Highway Administration 2014). The use of pavement temperature information is becoming more widespread with technological advancements (NCAR 2011) and emphasis on weather risk assessment and decision-support initiatives (e.g., Weather-Ready Nation; NOAA 2014). Rutz and Gibson (2013) recently provided a first-time perspective from the National Weather Service of incorporating pavement temperature forecasts and associated model results into decision-support applications. Earlier work (Hallowell and Blaisdell 2003) discussed the development of a prototype integrated maintenance decision-support system that considered pavement temperature among other variables to suggest a treatment recommendation to mitigate snow and ice accumulation on the road surface. As the use of pavement temperature forecasts becomes more widespread, one recurring source of forecast error is the influence of cloud cover (Bogren 1991). Clouds act to damp the diurnal variation of pavement temperatures, and existing models often have difficulty parameterizing such localized effects of cloud cover (Drobot et al. 2012); however, no attempts have been made to consider an independent cloud observation dataset with spatiotemporal resolution that would be sufficient for the purposes of forecasting applications. The current strategy to resolve this cloud problem in pavement temperature models is to produce a pavement forecast assuming complete cloud cover. This fails to consider more variable cloud situations such as partly cloudy or transitions from clear sky to cloud-covered sky (Drobot et al. 2012). Such a cloud correction, while not perfect, still does better than a clear-sky pavement temperature forecast. Still, greater refinement is needed

Corresponding author address: Curtis L. Walker, Bessey Hall Room 214, Department of Earth and Atmospheric Sciences, University of Nebraska–Lincoln, Lincoln, NE 68588-0340.
E-mail: curtis.walker@huskers.unl.edu

DOI: 10.1175/JAMC-D-16-0094.1

and there is a gap in the literature concerning issues of pavement temperature forecasts and subsequent decision-making.

One well-known model for pavement temperature forecasting is Environment Canada's Model of the Environment and Temperature of Roads (METRo; Crevier and Delage 2001). This model has the ability to forecast both the pavement temperature as well as the condition of the road surface based on initial conditions from both Road Weather Information System (RWIS) station data and the Canadian Meteorological Centre's Global Environmental Multiscale model. It is important to note that METRo can be coupled with any numerical weather prediction model (e.g., Weather Research and Forecasting Model). A 2007 study conducted by the National Center for Atmospheric Research (NCAR) found that the METRo generally outperformed similar pavement temperature forecasting models (NCAR 2007). A later NCAR study (Drobot et al. 2012) critiques the generally poor performance of METRo and those similar models under variably cloudy conditions. Their consensus was that surface energy balance models such as METRo were not accurate with respect to the radiative transfer influence of clouds because of numerous parameterizations and approximations that are used in such models. The primary METRo parameterization for cloud cover considers the cloud area fraction (i.e., observed station octets of cloud cover), which provides a sense of overall cloud cover but not the specific type of cloud that is influencing the radiative transfer and surface energy balance relationships. The METRo is capable of ingesting more specific cloud parameters (i.e., cloud thickness, cloud height) from other models; however, the challenge remains to obtain high-quality cloud information in the first place.

The radiative transfer impact of cloud cover has been assessed on several spatiotemporal scales (Stephens 2005). The research presented in this paper is focused on the radiative properties of clouds on short time periods and small spatial scales. Clouds influence radiative transfer in both the shortwave and longwave radiation spectrum. Downwelling shortwave radiation and cloud impacts on shortwave radiation, hereinafter referred to as ''surface radiation,'' can be summarized via a matrix of cloud types that focuses on the parameters of optical thickness and cloud-top height (Stephens and Tsay 1990; Várnai and Davies 1999; Chen et al. 2000). Thicker, lower clouds, which usually contain more liquid water, tend to reduce surface radiation more than higher, thinner mixed or ice phased clouds.

Observational studies and radiative transfer models, such as the Santa Barbara Discrete Ordinate Radiative Transfer (DISORT) Atmospheric Radiative Transfer Model (SBDART; SBDART 2013; Ricchiazzi et al. 1998), have shaped our present knowledge of cloud radiative forcing. Radiative transfer models provide a simulated approach to understanding how radiation interacts with atmospheric constituents. Real observations provide a ground truth to compare and improve such models. These observations are often obtained from satellite-based platforms. Real-time observations of such cloud properties yield the opportunity to identify and classify clouds based on those same properties. Several studies have developed, evaluated, and improved satellite-based cloud detection and classification algorithms such as the Moderate Resolution Imaging Spectroradiometer (MODIS) cloud mask algorithm (Ackerman et al. 2008) and the whole-sky infrared cloud-measuring system (WSIRCMS; Liu et al. 2011). Ground-based cloud identification is possible (Yang et al. 2012) as well, though the spatial extent is limited for applications such as pavement forecasting. Satellite technology provides continuous global coverage. The Naval Research Laboratory (NRL) Cloud Classification (NRLCC) algorithm applied to imagery from the operational National Oceanic and Atmospheric Administration's Geostationary Observational Environmental Satellites (NOAA–GOES; Bankert 1994; Tag et al. 2000; Bankert and Wade 2007; Bankert et al. 2009) is a near-real-time, postprocessing algorithm selected for the current analysis. The goal of this research is to develop a method for spatiotemporally matching NRLCC algorithm output through statistical methods with pavement temperature and surface radiation observations to develop a quantitative understanding of the influence of clouds. Such results may be used in future research to directly improve pavement temperature forecasts. The results of these analyses will serve as a foundation for eventual assimilation of these relationships and satellite-based cloud information directly into pavement temperature models.

2. Methods

Pavement temperature, surface radiation, and cloud types were obtained during the month of June 2011 primarily because of data availability; this time period allowed for relatively uniform solar radiation (i.e., consider solar angle) and there was spatiotemporal data consistency. Daytime hours are the primary daily time period of interest given the research objective of understanding the role of clouds in influencing surface radiation and pavement temperatures. It is important to first understand daytime shortwave radiation because it allows for the development of methods that can then be applied to the additional complexities presented by

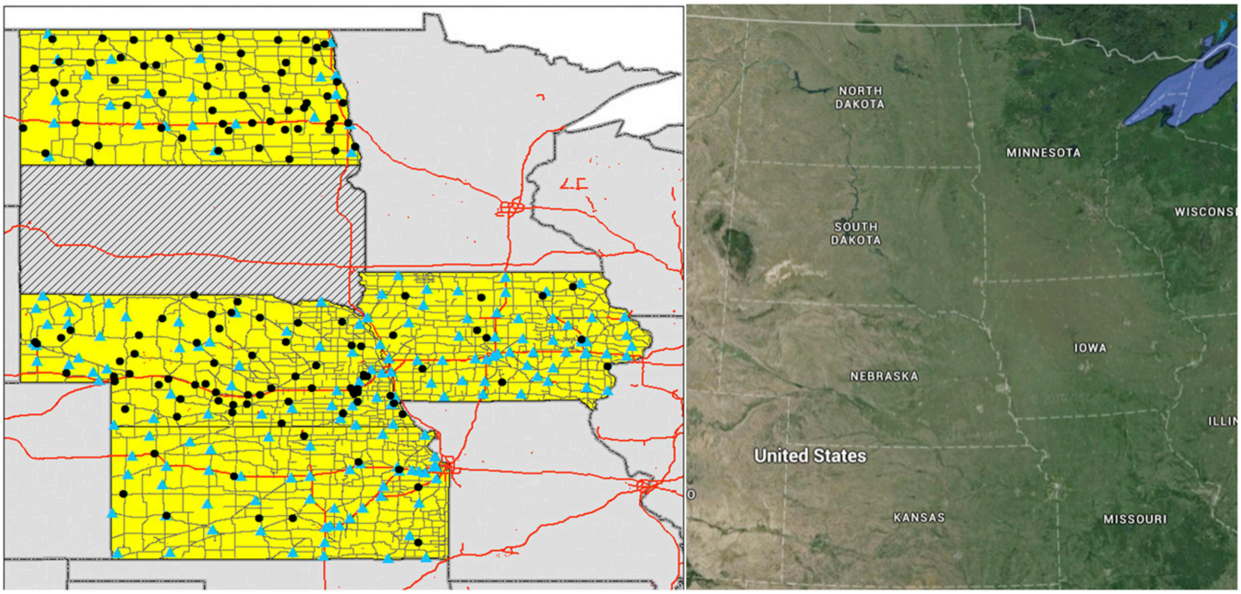

FIG. 1. (left) Study region; yellow states are those whose observations and data are used in the analyses. High Plains Regional Climate Center's AWDN stations (black dots) provide high-quality surface radiation observations. MADIS RWIS stations (blue triangles) provide pavement temperature data throughout the study region with primary and secondary roadways also marked within the study states. South Dakota is hatched to indicate that it was removed because of data inconsistency. (right) Landform image, copyrighted by Google Earth.

consideration of longwave radiation in future assessments. Further, the literature has shown that cloud cover most influences daytime pavement temperatures (Bogren 1991).

a. *Study region and data*

This study required a region that was both viewable by a single geostationary satellite for spatial consistency and contained a comprehensive meteorological surface data network for both surface radiation data and pavement temperatures. For these reasons, the study region for this work was defined by the state boundaries of North Dakota, Nebraska, Kansas, and Iowa (Fig. 1). Hourly surface radiation data (Changnon et al. 1990) were obtained from the High Plains Regional Climate Center's Automated Weather Data Network (AWDN; High Plains Regional Climate Center 2013). This network provides observation points spread throughout the Great Plains. Surface pavement temperature data were obtained via the National Oceanic and Atmospheric Administration's Meteorological Assimilation Data Ingest System (MADIS 2014) archived at the NCAR High Performance Storage System (HPSS; NCAR 2014). Because of a lack of reported pavement temperature data to MADIS, South Dakota was not included in the study region. MADIS pavement temperature data are measured from RWIS stations throughout the study region with a temporal resolution of approximately 10 min. There are approximately 175 RWIS stations included in this analysis. Cloud-type detection based on the NRLCC algorithm (NRL 2013) was also obtained from the NCAR HPSS. The temporal resolution of NRLCC algorithm is 15 min. The combination of visible and infrared satellite channels from GOES imagery allows for 4-km spatial resolution. These data were matched spatiotemporally with RWIS station observations.

b. *Analysis of clouds and pavement temperature*

The second step in the analysis is to observe and quantify the role of clouds on influencing surface radiation and subsequent pavement temperatures in an applied setting. It is necessary to isolate and extract the NRLCC algorithm output from the satellite pixels containing and surrounding the pavement temperature sensor. The pixel containing the pavement temperature sensor and the surrounding eight pixels are identified and their cloud-type information extracted (Fig. 2). This nine-pixel box (3×3 pixels) provides 12-km resolution of pavement temperature related to cloud-type group. This resolution is acceptable given the spatial distribution of RWIS stations throughout the study region and the fact that cloud-type groups are generally spatially consistent (Hartmann et al. 1992; Chen et al. 2000). Then, for each time stamp, the clouds are grouped into general types based on height characteristics (Table 1), and the most frequent of the general cloud types for all nine pixels is assigned to the surface observation for the

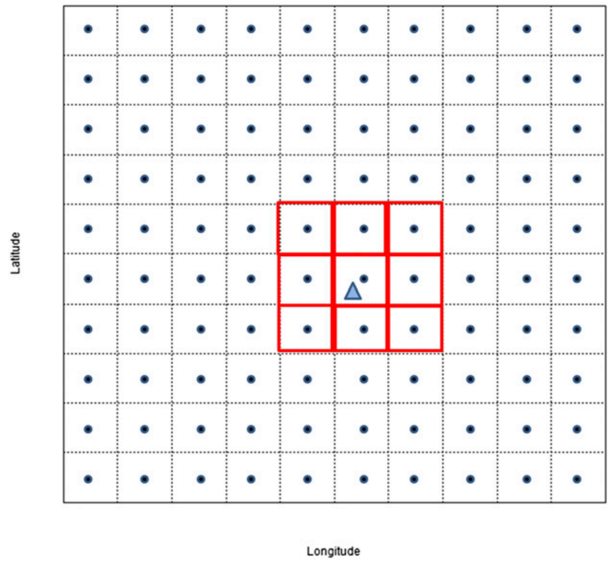

FIG. 2. Schematic of method to spatially relate pavement temperature sensors (blue triangle) with NRLCC algorithm data. The gridcell spacing is 4-km resolution and each centroid represents a longitude–latitude coordinate pair from the NRLCC algorithm. The red boxes denote the pixels selected for extracting cloud information, which includes the pixel containing the pavement temperature site as well as the surrounding pixels.

time stamp. This is termed the "modal cloud." Hereinafter these modal cloud assignments will be referred to as cloud-type groups.

For quality control purposes, the following criteria are imposed on individual pavement temperature sites on a state-by-state daily basis. At the state level, a mean pavement temperature is computed for the pavement temperature time series along with associated standard deviations for a single day. A site was removed from the dataset if more than 50% of its observations are greater than two standard deviations from the mean in any of the following three time periods on that particular day: 0000–1159, 1200–2359, or 0000–2359 UTC. This process was repeated each day for all states to identify if particular sites experienced a malfunction for a period of time or if something anomalous occurred. Although nocturnal cloud observations are not considered in this analysis, the overnight time period is still used in the quality control criteria to have a more stringent requirement on the entire dataset. A "bad" site at night might have some measurement error that would propagate into the daytime as well, though it may be masked by a day with a complex cloud-type group assortment. It is important to note that throughout the dataset, sites that violated the criteria did so for an extended period of time. There were very few instances in which a site was marginal in terms of adherence to the quality control

TABLE 1. Cloud-type groups arranged by height for the analysis.

Cloud-type groups			
Low	Middle	High	Cumuliform
Stratus	Altocumulus	Cirrus	Cumulus
Stratocumulus	Altostratus	Cirrostratus	Cumulus congestus
		Cirrocumulus	Cumulonimbus
			Cirrostratus anvil

criteria. There tended to either be a noticeable violation or the site was deemed appropriate to remain in the analysis.

c. Case study selection

After matching cloud observations to those of pavement temperatures and considering the dataset as a whole, it was desirable to consider a smaller subset of the data for more detailed analyses. For the purposes of data continuity, the period of 1–16 June 2011 was parsed from the June 2011 dataset. This allowed for just over two weeks of pavement temperature observations to be compared with the month as a whole to ensure that the subset was representative of the variability among cloud cover and pavement temperature. These 16 days were then classified as either clear or cloudy based on whether or not a simple majority of pavement temperature observations had a modal cloud classification of clear or some type of cloud cover present (Table 2). For later analyses 1 June was further subdefined as a partly cloudy day given the nearly equal number of cloud versus clear observations, 6 June was deemed a representative clear day, and 9 June was deemed as a representative cloudy day. While 6 June was the day with the highest number of clear observations, 9 June was the day with the second-largest number of cloudy observations. The cloudiest day, 2 June, was not selected as the representative cloudy day as there were data discontinuities. These three days will be used in subsequent cross validation to rate the overall success of the algorithm and spatial association.

After defining representative case study days and a smaller subset, a method to remove diurnal dependence was defined. The aforementioned June 2011 distribution analysis comparisons did not remove diurnal or daily variabilities. For example, a particular day could have higher pavement temperatures than another because of synoptic meteorological conditions (e.g., cold front passage). A simpler example is to compare time of day (TOD). Morning sunrise is associated with cooler temperatures than midday peak solar heating. For a less biased comparison of the data, observations were

TABLE 2. Number of pavement temperature observations 1–16 Jun 2011 defined as either clear or cloudy and declaration for each day.

Date (June 2011)	Clear obs (%)	Cloudy obs (%)	Day classification
1	2103 (51.0)	2024 (49.0)	Clear
2	558 (13.2)	3680 (86.8)	Cloudy
3	2368 (58.3)	1691 (41.7)	Clear
4	1820 (27.4)	4821 (72.6)	Cloudy
5	3194 (84.1)	605 (15.9)	Clear
6	4212 (93.5)	295 (6.5)	Clear
7	5140 (89.8)	585 (10.2)	Clear
8	4910 (73.4)	1779 (26.6)	Clear
9	1242 (21.2)	4631 (78.8)	Cloudy
10	1000 (24.0)	3167 (76.0)	Cloudy
11	1571 (38.8)	2476 (61.2)	Cloudy
12	1280 (30.9)	2864 (69.1)	Cloudy
13	1530 (39.4)	2351 (60.6)	Cloudy
14	1227 (31.1)	2718 (68.9)	Cloudy
15	2551 (67.4)	1233 (32.6)	Clear
16	2075 (51.6)	1944 (48.4)	Clear

TABLE 3. Matched (12-km threshold) AWDN and RWIS sites (MP indicates milepost).

Site No.	AWDN	RWIS
1	Hofflund, ND	Ray, ND, U.S.-2 MP 51.3
2	Wishek, ND	Wishek, ND, ND-3 MP 40.7
3	Fargo, ND	Fargo, ND, I-94 railroad bridge
4	Bowman, ND	Bowman, ND, U.S.-85 MP12.2
5	Mandan, ND	Bismarck, ND, I-94 bridge
6	Scottsbluff, NE	Highway 71 south of beltline
7	Halsey, NE	Dunning–Middle Loup Bridge
8	Newport, NE	Newport, NE, on Highway 20 at MP 273
9	Cedar Rapids, IA	Cedar Rapids, IA, U.S.-30
10	Garden City, KS	U.S.-50 at K-156 bridge
11	Manhattan, KS	K-177
12	Silverlake, KS	I-470 bridge over U.S.-75
13	Silverlake, KS	U.S.-75

rearranged and compared on the basis of TOD. Five key TODs were defined for each day in the period of 1–16 June 2011: sunrise (1200 UTC), morning (1500 UTC), midday (1800 UTC), afternoon (2100 UTC), and sunset (0000 UTC). These time periods were defined by whether or not the NRLCC algorithm was in its day or night mode. Sunrise and sunset were identified based on the first available time stamp in which all sites throughout the study region did not observe a nighttime cloud observation. It is important to note that this induces about a 1-h difference in the amount of sunlight across the study region. For example, a site in the eastern part of the study region will have had daylight for an hour, whereas a site in the western part of the study region would only have sunlight for a few minutes. Three-hour increments were then used to establish the remaining three TODs. Typical peak solar heating occurred between midday and afternoon. Time series and distribution analyses for each cloud-type group were analyzed at each TOD. Hourly distributions were also computed to compare the pavement temperature distribution throughout the day for each cloud-type group. The advantage of removing the diurnal trend allows for a less biased comparison of the pavement temperature and cloud-type group observations; however, synoptic trends and localized station biases within the dataset are also revealed.

d. Identification of correlation among clouds, pavement temperature, and radiation

Surface radiation observations from AWDN sites were included in the analysis based on the proximity between RWIS and AWDN sites. A spatial threshold of 12 km was used to be consistent with the same spatial resolution of matching RWIS sites with NRLCC algorithm cloud output (Fig. 2). Based on the spatial threshold criterion, 17 total pairs of matched AWDN and RWIS sites were identified, though data inconsistencies reduced this number to 13 sites (Table 3). Similar to the pavement temperature and cloud-type group analyses, distributions of surface radiation among the cloud-type groups were considered only at the specific TODs to remove diurnal and sun angle bias for more meaningful comparisons and discussion.

Correlation and other statistical analyses were performed to measure the relationships among cloud-type groups, pavement temperatures and surface radiation observations. These analyses were performed for the 1–16 June 2011 period on all 13 sites rather than the individual case study days or individual sites because of the relatively small sample size. The statistical analyses were considered for each TOD.

e. Cross validation: Cloud identified versus satellite imagery

Archived GOES visible satellite images were obtained from the NOAA Comprehensive Large-Array Data Stewardship System (CLASS 2014). These 1-km spatial resolution images were cross examined with the NRLCC algorithm output. The intent was to provide a preliminary, qualitative feasibility assessment of the output from the NRLCC algorithm. The CLASS archived visible satellite images were spatiotemporally matched with algorithm output for the three case days (1 June, partly cloudy; 6 June, clear; 9 June, cloudy). The RWIS locations were plotted on the visible satellite image and color coded according to the cloud-type groups identified by the NRLCC algorithm. This cross-examination

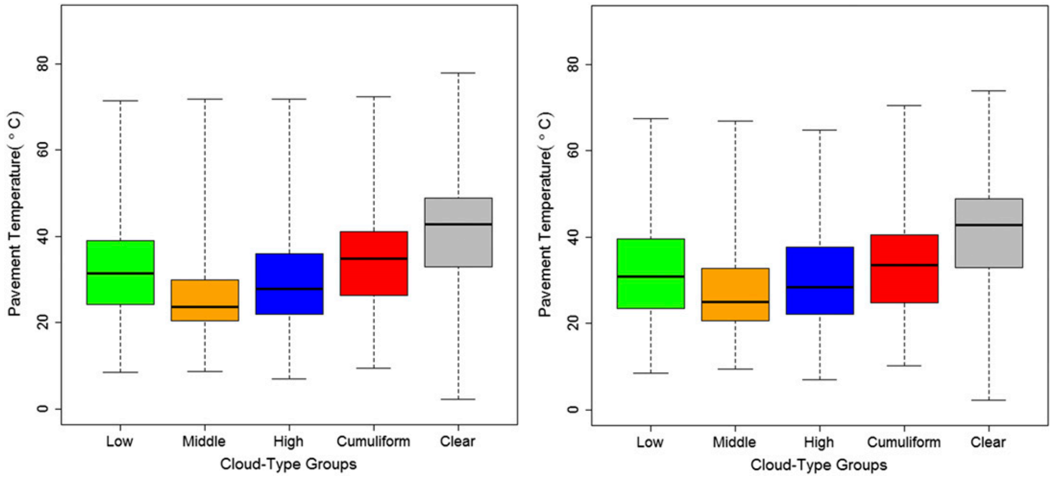

FIG. 3. (left) June 2011 road pavement temperature distributions sorted by cloud-type groups and (right) road pavement temperature distributions during 1–16 Jun 2011 sorted by cloud-type groups: low (green), middle (orange), high (blue), cumuliform (red), and clear (gray). The whiskers represent the extremes for the data (i.e., minimum and maximum), the box represents the first and third quartiles (interquartile range), and the median is the black bar in the middle of each box.

assessment can also be considered a check on the nearest pixel-matching method between NRLCC algorithm output and the RWIS sites.

3. Results and discussion

a. Overall cloud–pavement temperature distribution

The research objective was to quantify the influence of cloud-type groups on both pavement temperature and surface radiation. The June 2011 pavement temperature distributions by cloud-type group are similar to those of the 1–16 June 2011 distributions (Fig. 3) and median pavement temperature time series (Fig. 4). The similarities between the two time periods suggest that, despite variations in sample size between the whole month and first two weeks, there are effects from cloud cover on pavement temperatures (Table 4). Further, the similarities of these two datasets support use of the two-week data for more detailed analyses. The entire June 2011 dataset contained several days of missing data toward the end of the month. While it was desirable to note such data discontinuities did not impact the overall pavement temperature distributions, opting for a more consistent data period during the first 16 days was desirable for the remainder of the analysis. The low cloud-type group (i.e., stratus and stratocumulus) is in the middle for pavement temperature and had one of the largest interquartile ranges (IQR). Low clouds tend to occur most often in the morning associated with morning fog, though they are also associated with precipitation during the day as well.

The cumuliform cloud-type group (i.e., cumulus, cumulus congestus, cumulonimbus, and cirrus anvil associated with deep convection) presents a challenge of its own because of the scattered nature of the clouds. Cumuliform clouds contained the second-highest pavement temperatures after clear-sky conditions when considering the median distribution for the entire month and two-week data. The cumuliform cloud-type group contains some of the most complicated cloud situations.

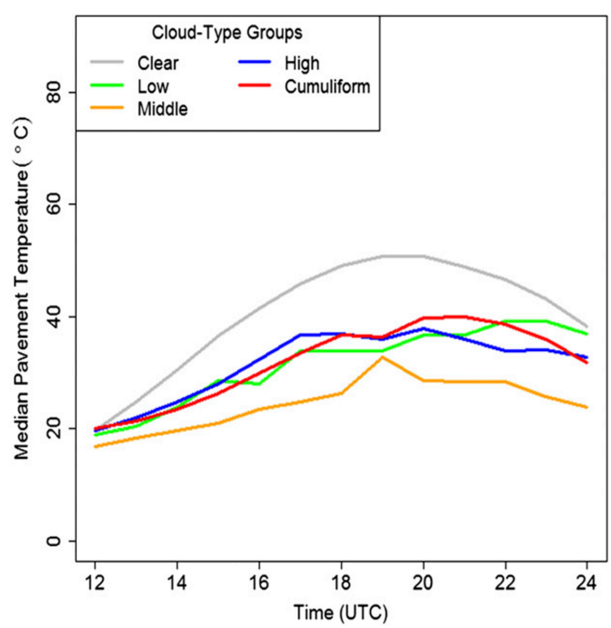

FIG. 4. Hourly 1–16 Jun 2011 median pavement temperature observations colored by cloud-type groups.

TABLE 4. June 2011 and 1–16 Jun 2011 pavement temperature distribution analyses results.

Cloud-type group	No. of obs	Mean road temperature (°C)	Median road temperature (°C)	IQR (°C)
		June 2011		
Low	11 603	32.1	31.5	14.8
Middle	10 638	25.8	23.7	9.5
High	18 492	29.4	27.9	14.1
Cumuliform	18 470	34.2	34.9	14.8
Clear	51 852	40.9	42.8	15.9
		1–16 Jun 2011		
Low	8530	31.8	30.9	16.2
Middle	5755	27.1	25.0	12.1
High	12 059	30.0	28.4	15.7
Cumuliform	10 520	33.3	33.5	15.6
Clear	36 781	40.8	42.9	16.0

Fair-weather cumulus clouds can be very scattered in nature shading only some regions from direct sunlight, whereas deep convective clouds can be spatially broad and opaque to sunlight, yielding cooler pavement temperatures. This combination of factors explains why the cumuliform cloud-type group exhibits the second-highest pavement temperature and one of the larger IQR. If the cumuliform clouds identified are more of a spatially scattered cumulus higher pavement temperatures would be observed; however, if a thicker cumulonimbus type of cumuliform is identified pavement temperatures would be lower. As expected, clear pavement temperatures are the highest, especially given the time of year. The important distinction to note is that clear pavement temperatures range anywhere from 6° to 15°C higher than their cloud counterparts. Extrapolate this difference to a wintertime scenario in which increasing or decreasing cloud cover could have substantial ramifications for a pavement temperature forecast with the threat of frozen precipitation.

The middle cloud-type group (i.e., altostratus and altocumulus) contained the lowest median pavement temperature observations (Figs. 3 and 4). The middle cloud-type group also has the smallest IQR for both the June 2011 and 1–16 June 2011 periods, indicating that these clouds tend to have a less variable effect on pavement temperatures since middle clouds tend to be more spatially uniform. These results indicate that the effect of the middle cloud-type group on pavement temperature is consistent. Such cloud types tend to be more optically thick and encompass a broad spatial extent of the sky resulting in the lowest observed pavement temperatures and the least variability of pavement temperatures when they are present. The median time series curve for the middle cloud-type group (Fig. 4) likely has a noticeable increase in observed pavement temperatures at 1900 UTC because of the relatively low frequency of occurrence (i.e., small sample size) for that particular group.

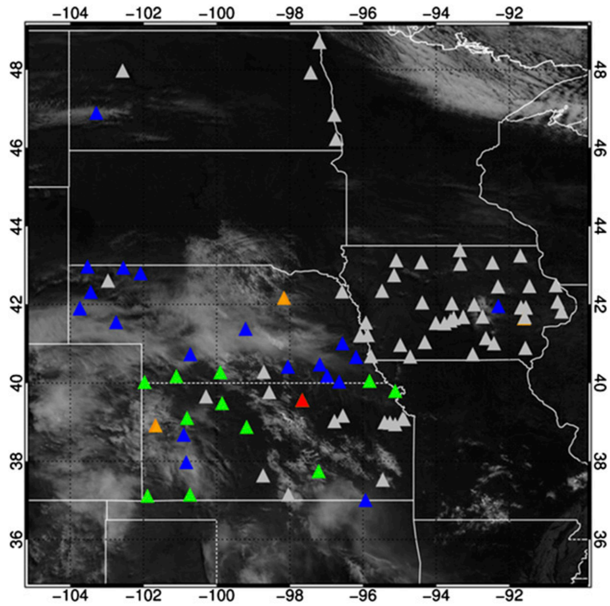

FIG. 5. Partly cloudy; 1500 UTC 1 Jun 2011 visible satellite imagery with NRLCC algorithm cloud-type group identified at RWIS sites overlaid.

High clouds (i.e., cirrus, cirrostratus, and cirrocumulus) contained the second-lowest median observed pavement temperature for the month and two-week data, which is somewhat unexpected. One might expect that given the relatively thin characteristics of the high cloud-type group, pavement temperature would more closely resemble those of clear skies. This is an indication of an important limitation of satellite-derived cloud observations. Downward-viewing satellites observe cirrus clouds first and may be unable to detect other cloud-type groups below a cirrus canopy. It is suggested that while some of the observed high cloud observations are truly only cirrus clouds, other situations are more suggestive of multiple layers of clouds and only the cirrus layer is detected. These multiple-cloud-layer situations provide a plausible explanation for the relatively low observed pavement temperature despite high clouds generally being more transparent to solar radiation.

b. *Cross validation: Satellite imagery versus observed cloud cover*

Satellite cross validation reveals that the NRLCC algorithm generally performs quite well despite complex cloud situations, although there are some apparent limitations with multilevel cloud scenarios (Figs. 5 and

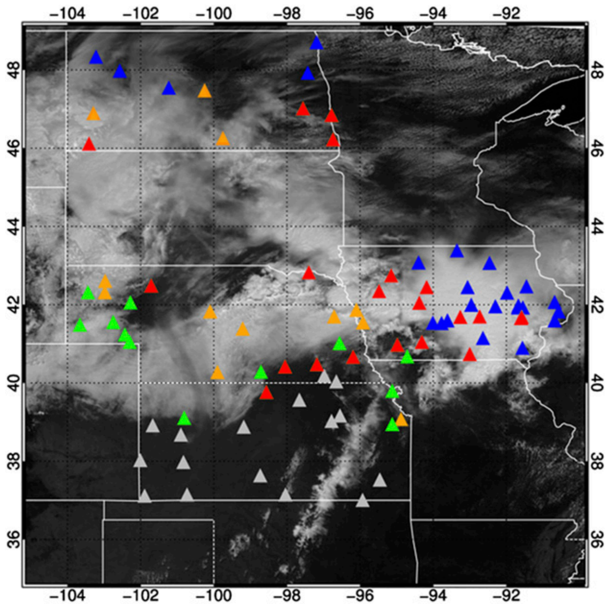

FIG. 6. Cloudy day; 1800 UTC 9 Jun 2011 visible satellite imagery with NRLCC algorithm cloud-type group identified at RWIS sites overlaid.

6). On 1 June 2011, the partly cloudy case day, how well the NRLCC algorithm output transitions with different cloud-type groups is observed. In the morning (Fig. 5), North Dakota is clear except for some high clouds identified in the southwestern corner of the state. Similarly, Iowa is mainly clear as well except for some high and middle clouds identified in the eastern part of the state. Kansas and Nebraska contain a far more complex cloud situation. A cirrus cloud deck is apparent in both visible imagery and algorithm output in eastern Nebraska. Lower clouds are identified southwest of this cirrus deck along the Kansas–Nebraska border. It is somewhat difficult to determine whether or not these low clouds are in fact more of a cumuliform, perhaps stratocumulus cloud given the localized areal extent. Such NRLCC algorithm output confusion could explain similarities in the median time series among cumuliform and low cloud-type groups (Fig. 4).

On 9 June 2011 (Fig. 6) in Nebraska low clouds are generally identified in the western part of the state, middle in central Nebraska, and cumuliform clouds in the east. This zonal classification of cloud-type groups is typical of what is associated with a cold frontal passage. Cumuliform clouds will be associated with convection and transition to more of a stratiform shield associated with the relatively cooler, drier air mass in the postfrontal environment. A more mesoscale situation is apparent in the cloud-type groups identified in Iowa. Deep convection in the western part of the state is associated with cumuliform clouds, whereas the cirrus anvil from this convection is identified as high clouds over eastern Iowa. It is important here to note that there are likely lower cloud layers beneath the cirrus anvil that cannot be detected from the satellite-based NRLCC algorithm. North Dakota's cloud situation is once again suggestive of the synoptic situation with high clouds in the northern part of the state yielding to likely thicker, more spatially uniform and consistent middle and cumuliform cloud-type groups in the southern part of the state.

In this feasibility assessment, the NRLCC algorithm output and RWIS pixel-matching method generally align quite well with visible satellite imagery for a variety of locations, areal extents, and cloud situations. Some important caveats to note include the likelihood that high cloud-type group identification must be considered in context with the atmospheric situation. On the partly cloudy day (Fig. 5), the high cloud (cirrus arc over Nebraska) is less likely to be associated with cloud layers below (given the thin, wispy visible image appearance) than the high clouds on the cloudy day (Fig. 6) associated with convection.

c. *Cloud–pavement temperature analyses*

A time series of median pavement temperature observations by cloud-type groups exhibits a clear distinction between cloudy conditions and clear conditions (Fig. 4). Among the four cloud-type groups, the middle cloud has the lowest median time series. This signifies that the radiative properties of such cloud groups are important to model distinctly rather than grouping all clouds together. Recall that Drobot et al. (2012) considered a strategy to improve pavement forecasts in which conditions were simply assumed to be completely overcast (i.e., 100% cloud cover). Such a strategy does not consider the unique influence of more specific cloud-type groups as observed in the median pavement temperature time series. It could be suggested that a similar model may be appropriate for the cumuliform, low, and high cloud-type groups combined given their similar median pavement temperature curves. It is also important to note the observed increased variability of the median pavement temperature time series from morning through evening. Other factors such as the aforementioned discussion of multiple cloud layers and difficulty distinguishing between low stratocumulus type clouds and other low-level cumuliform cloud types could explain why the median time series for the low, high, and cumuliform cloud-type groups (Fig. 4) are more closely related than the median time series of clear or middle clouds. The NRLCC algorithm is superior at distinguishing cloud from clear, though there may be situations in which the further subdivisions introduce error into the identification.

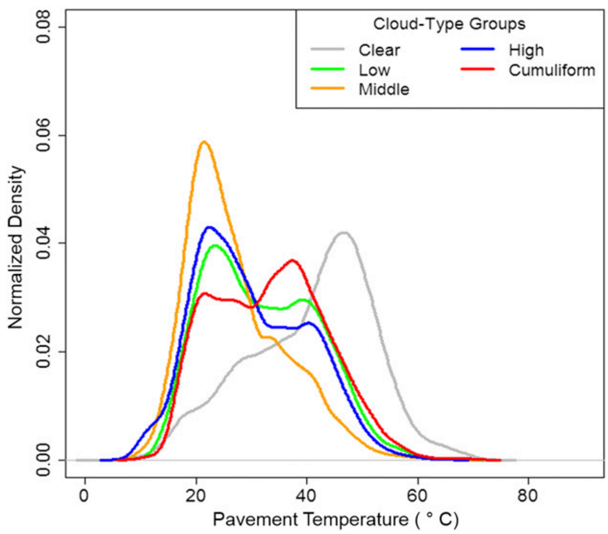

FIG. 7. Gaussian kernel density distribution for 1–16 Jun 2011 pavement temperatures colored by cloud-type group. The *y* axis is normalized to provide relative frequency distribution among the cloud-type groups.

For the 1–16 June 2011 period, another method to compare pavement temperature distributions by cloud-type group is with a probability density (Fig. 7). At lower pavement temperatures there is a greater density, and therefore higher probability, of a particular observation being associated with cloud cover. At higher pavement temperatures, there is a greater propensity for clear observations. It is also important to note that cloud-cover pavement temperature distributions do appear to be somewhat bimodal with a weaker, secondary peak occurring at higher temperatures. This is likely due to the time of day at which any given cloud-type group occurs. Cloud cover during the peak solar heating of any given day will still yield higher pavement temperatures than, for example, an early morning or late evening cloud cover. This bimodal nature is substantially more apparent in the cumuliform cloud-type group, which agrees with the aforementioned discussion of how this group represents the most complex cloud situations. Lower pavement temperatures with cumuliform clouds are likely associated with deep convection. Higher pavement temperatures with the same cloud-type group are more likely to occur in situations with fair-weather, scattered cumulus clouds. This cloud-type group has a higher probability of such split observations.

The TOD distribution analyses (Figs. 8 and 9) best illustrate the impact of the cloud-type groups on pavement temperatures and surface radiation. Recall the five key TODs that were defined: sunrise (1200 UTC), morning (1500 UTC), midday (1800 UTC), afternoon (2100 UTC), and sunset (0000 UTC). A discussion of the tendencies of pavement temperature and surface radiation cloud-type groups at each time step allow for quantification of the impact of cloud type on pavement temperature and surface radiation (Fig. 8). At 1200 UTC, or approximately sunrise, the lowest daytime temperatures are observed for all groups. Further, the surface radiation distributions are very similar with little variation as well (Fig. 10), which correlates to the concept of the day–night transition energy balance equilibrium state that was also observed in the pavement temperatures. This suggests that near the day–night transition, the variability in pavement temperature associated with cloud cover is at quasi equilibrium, illustrating the radiative balance between shortwave radiation and longwave radiation. Despite the similarities, it is important to note that while there is little surface radiation near sunrise, there already is some separation among clear and cloudy conditions.

Moving ahead to 1500 UTC (morning), the solar zenith angle decreases (i.e., sun rises higher in the sky) and the pavement temperatures for cloud-type groups begin to differentiate between clear versus cloud. Clear conditions, not surprisingly, observed the most rapid increases in pavement temperatures of 16.7°C between the two TOD. The four cloud-type groups increased in temperature as well; however, there was a clear reduction in the magnitude of increase. Low-cloud pavement temperatures observed the second-highest increase of 9.6°C, followed by high-cloud pavement temperatures with 8.3°C; cumuliform cloud-type group at 6.4°C and middle-cloud pavement temperature observations increased the least, with only a 4.2°C increase in the median. There is substantially more division among the surface radiation distributions by cloud-type group (Fig. 10). The cumuliform cloud-type group observed a similar increase to that of high clouds, whereas low and middle clouds were similar to one another. These results suggest that the radiative influence of optically thin high clouds is similar to that of spatially scattered (albeit optically thicker) cumuliform clouds. Low and middle cloud-type groups tend to be both optically thicker and more spatially uniform and consistent, hence their lower observed median surface radiation.

Peak solar heating typically occurs around midday (1800 UTC) although the highest pavement temperatures should occur after this TOD. The lagged response of the pavement temperature to solar heating is associated with the specific heat capacity of the atmosphere, thermal inertia of the road surfaces and the fact that the surface remains exposed to warming for several hours after peak solar heating. Substantial energy is required to affect the sensible heat of any given material such as a

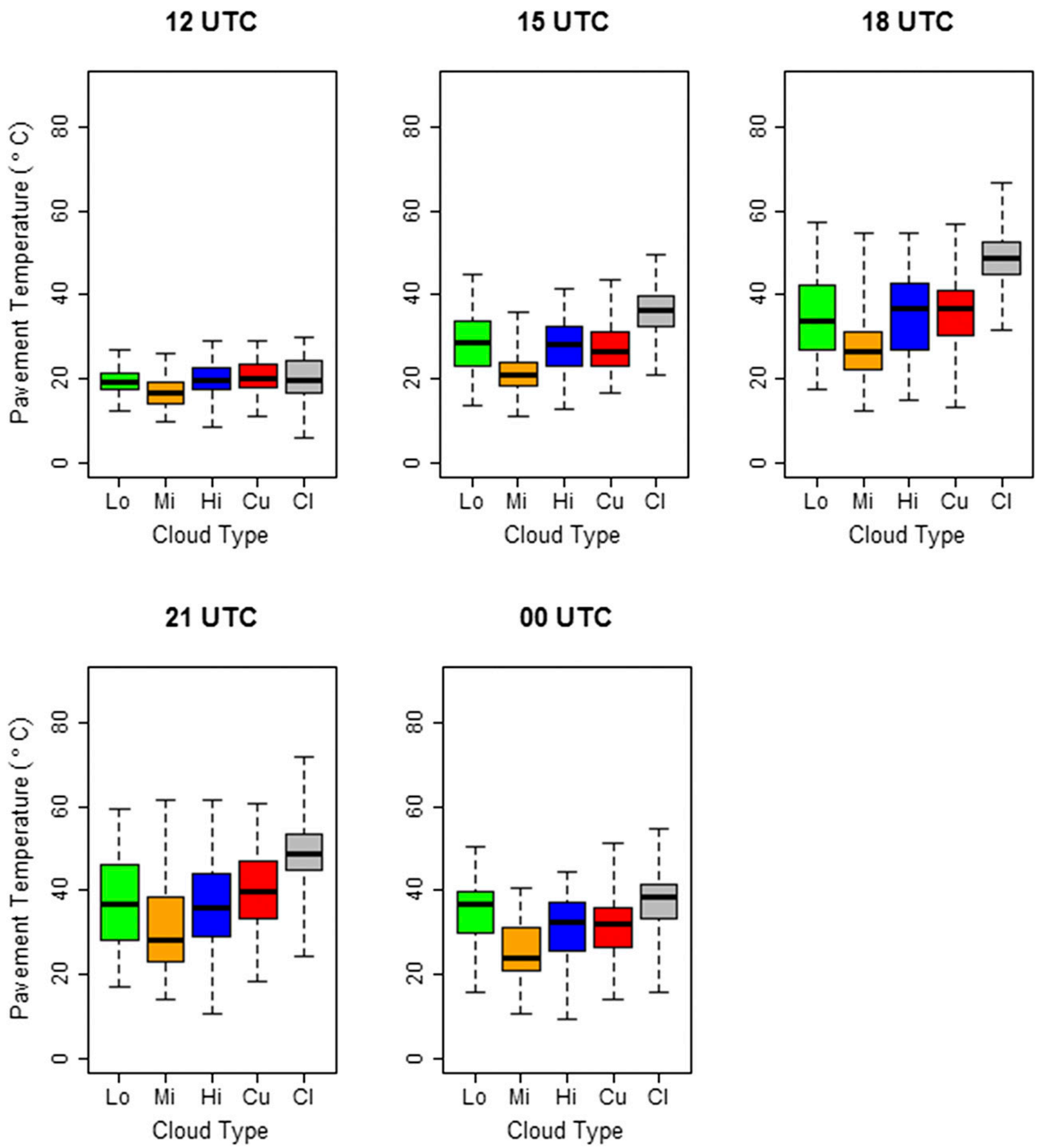

FIG. 8. TOD pavement temperature observation distributions for 1–16 Jun 2011 stratified by cloud-type groups: low (green), middle (orange), high (blue), cumuliform (red), and clear (gray). 1200 UTC represents approximate sunrise, 1500 UTC is a morning observation, 1800 UTC represents the middle of the day in which typical peak solar heating occurs, 2100 UTC is the afternoon, and 0000 UTC represents approximate sunset. The whiskers represent the extremes for the data (i.e., minimum and maximum), the box represents the first and third quartiles (interquartile range), and the median is the black bar in the middle of each box.

road. An important difference among the pavement temperature distributions and those for surface radiation is that peak radiation observations are much closer to peak solar heating (1800 through 1900 UTC), whereas peak pavement temperatures were more likely to occur between 1900 and 2100 UTC. Similar to the tendencies in pavement temperature, surface radiation for clear conditions has the fastest increase in the morning,

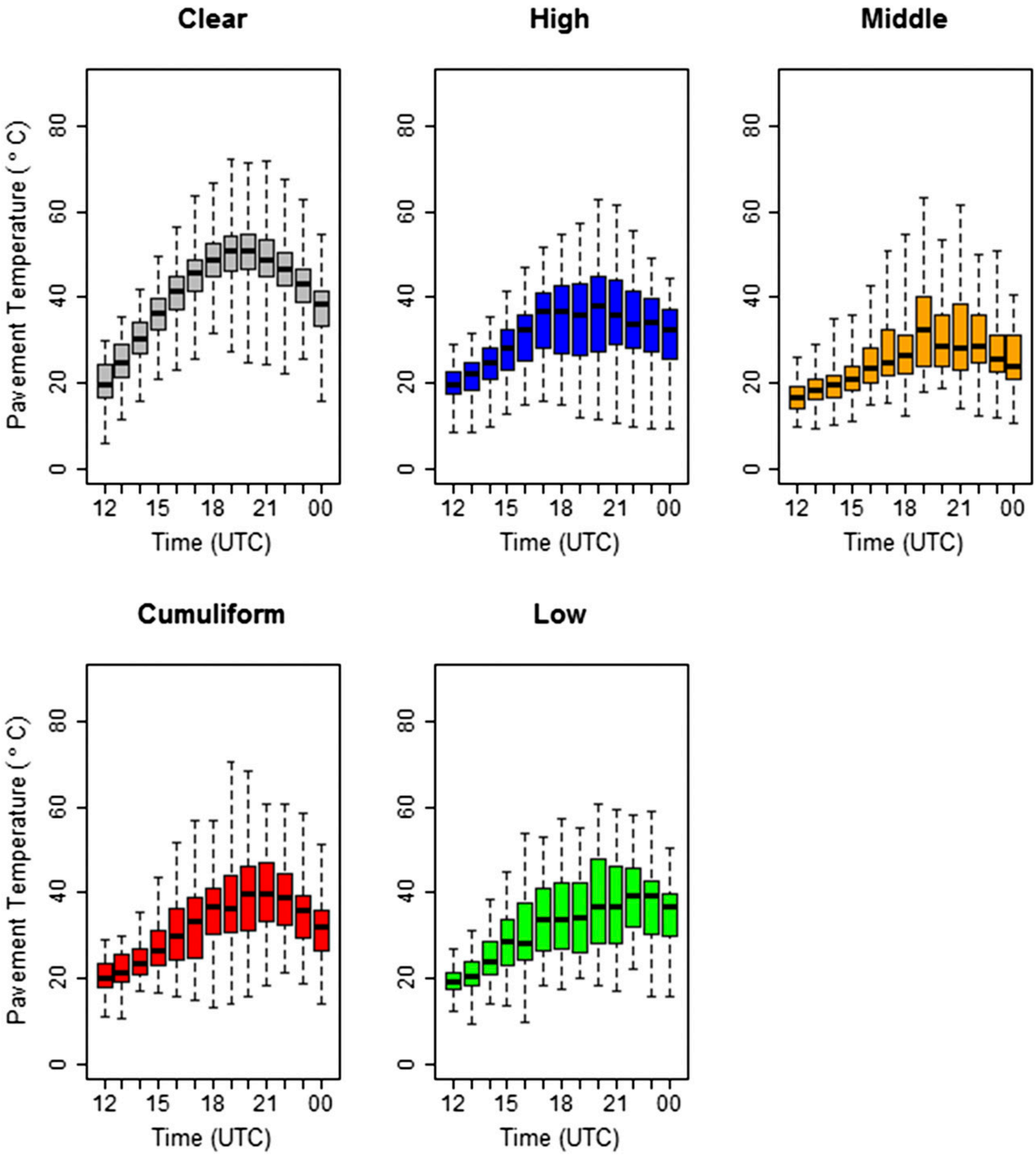

FIG. 9. Hourly pavement temperature distributions for the 1–16 Jun 2011 period sorted by cloud-type groups. The whiskers represent the extremes for the data (i.e., minimum and maximum), the box represents the first and third quartiles (interquartile range), and the median is the black bar in the middle of each box.

whereas surface radiation under the cloud-type groups catches up during the midday period.

The afternoon period (2100 UTC) generally observed the highest median pavement temperatures associated with all cloud-type groups and relatively small increases from the midday TOD. Interestingly, pavement temperatures decreased slightly for clear conditions and increased for the cloud-type groups. One possible reason for the increase in pavement temperatures associated with cloud cover and decrease for clear-sky

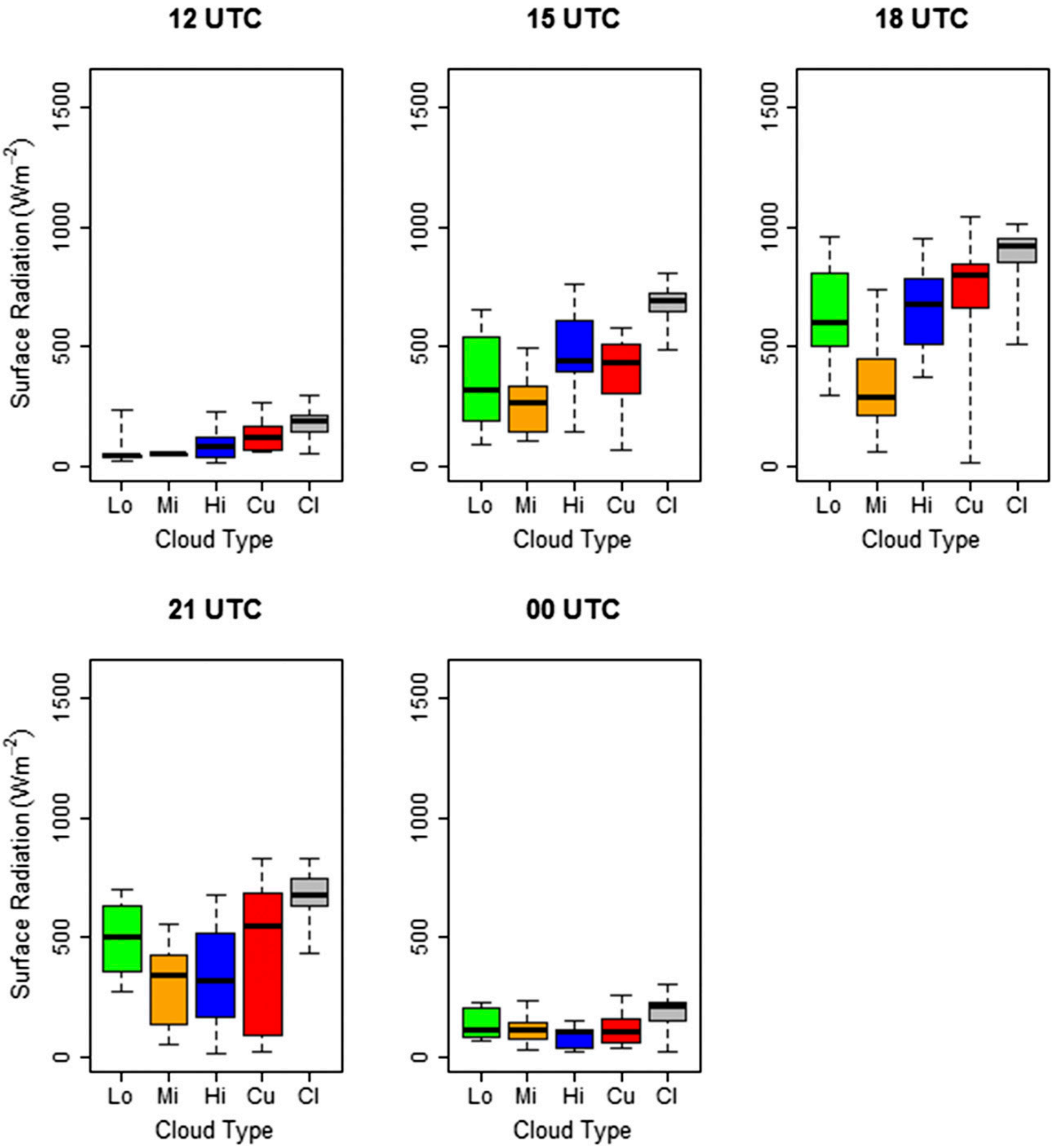

FIG. 10. As in Fig. 8, but for surface radiation.

pavement temperatures is that clouds impede both longwave and shortwave radiation from traversing into space. Cloud cover will act to keep pavement temperatures cooler than clear-sky pavement early in the day and then will act to keep pavement temperatures slightly elevated later in the day. Surface radiation observations generally tend to decrease as solar zenith angle increases (Fig. 10). Cumuliform cloud-type group radiation decreases faster than clear conditions, whereas low cloud-type group radiation values do not decrease as quickly. The high cloud-type group observes the most rapid decrease in surface radiation during the period. Such a rapid decrease with such a relatively optically thin cloud-type group seems anomalous. The rapid decrease of radiation associated with the cumuliform cloud-type group can similarly be attributed to more optically thick and spatially robust cumuliform clouds during afternoon deep convection (Fig. 6). These results also support developing future pavement temperature forecasts not based solely on adjustments to surface radiation but considering a direct adjustment to pavement temperatures given cloud identification.

At sunset (0000 UTC) there is a decrease for all pavement temperature cloud-type groups. Just as quickly as it climbed, pavement temperatures associated with clear conditions cool rapidly as well with an afternoon to sunset decrease of 10.6°C. Pavement temperature observations under the cumuliform cloud-type group cooled the second most rapid with a median decrease of 8.0°C. This is followed by middle clouds at 4.6°C and high clouds at 3.4°C. Low clouds observe a slight increase of 0.1°C from the afternoon TOD to the sunset TOD, which essentially represents no change. These results are likely associated with the fact that cloud cover damps the diurnal pavement temperature cycle. Pavement temperatures early in the day are kept cooler, whereas later in the day the pavement does not cool as quickly because of cloud cover insulating surface radiation. The surface radiation distributions by cloud-type group exhibit a return to quasi-equilibrium conditions associated with the day–night transition (Fig. 10). The 3-h differences in median radiation are not discussed below as the median values for radiation all approach approximately $100\,\mathrm{W\,m^{-2}}$ for all cloud-type groups and $200\,\mathrm{W\,m^{-2}}$ for clear conditions. An important distinction to note between the sunset periods for surface radiation versus that of pavement temperature is that pavement temperatures did not approach quasi equilibrium until some undetermined time after sunset (Fig. 8). This is also an important caution for future consideration of pavement temperatures after the day–night transition and accounting for the influence of longwave radiation.

Hourly pavement temperature distribution observations allow for an increase in the temporal resolution to consider the differences among the pavement temperature cloud-type groups (Fig. 9). The position of each cloud-type group in the figure is deliberate to suggest the cumuliform cloud-type group exhibits a hybrid tendency of clear and cloud conditions and the remaining cloud-type groups are more distinct. Clear pavement temperatures have the least within-period variation throughout the day and the most between-period variations. This is due to the fact that surface radiation is not impeded by cloud cover. Clear median pavement temperatures change rapidly with solar heating. Cumuliform and low cloud-type groups both exhibit reductions in pavement temperature from clear-sky pavement and also the largest within TOD variability. High cloud-type group observed pavement temperatures are lower than those of cumuliform and low cloud-type groups. Middle clouds observe the coolest and most damped diurnal median pavement temperature tendencies. These apparent relationships suggest some of the governing principles associated between cloud cover and pavement temperatures. Given the nature of the middle cloud-type group (i.e., altocumulus and altostratus) these tend to be some of the more optically thick clouds. Further, the middle cloud-type group tends to produce more of a uniform cloud deck over a given region. The high cloud-type group tends to be optically thinner in nature and so the pavement temperature response to this cloud-type group is not as severe as with that of the middle group. The cumuliform and low cloud-type groups contain the largest within-TOD variability because of the nature of these clouds. The cumuliform cloud-type group contains generally optically thick clouds; however, they may be very sparse and scattered in nature (e.g., fair-weather cumulus clouds) or quite dense (deep convective cumulonimbus clouds). A similar statement is applicable to the low cloud-type group, which may contain relatively optically thin stratus (i.e., fog) or widely scattered stratocumulus. Optically thicker clouds in the same low cloud-type group could be a denser and uniform layer of stratus clouds such as those associated with precipitation. These pavement temperature distributions represent the first time that satellite cloud data are used to develop cloud-type groups that can be associated with pavement temperature observations.

d. Relationships among cloud, pavement temperature, and surface radiation

Hourly surface radiation distribution observations allow for an increase in the temporal resolution to consider the differences among the surface radiation cloud-type groups (Fig. 11). Again, the position of each cloud-type group within the figure is deliberate to suggest that there are similarities among clear, cumuliform cloud-type group, and low cloud-type group. At 2000 UTC, clear conditions appear to have a minimum value of $0\,\mathrm{W\,m^{-2}}$. This denotes a possible limitation of these data as sensor malfunction or animal interaction such as a bird could interfere with data fidelity; however, it is important to consider the median observations and overall variation. Clear conditions have the least within-group variation throughout the day, while cumuliform and high cloud-type groups exhibit greater variability in the afternoon than in the morning (Fig. 11). As previously discussed, the increase in afternoon variability with these two cloud-type groups is likely associated

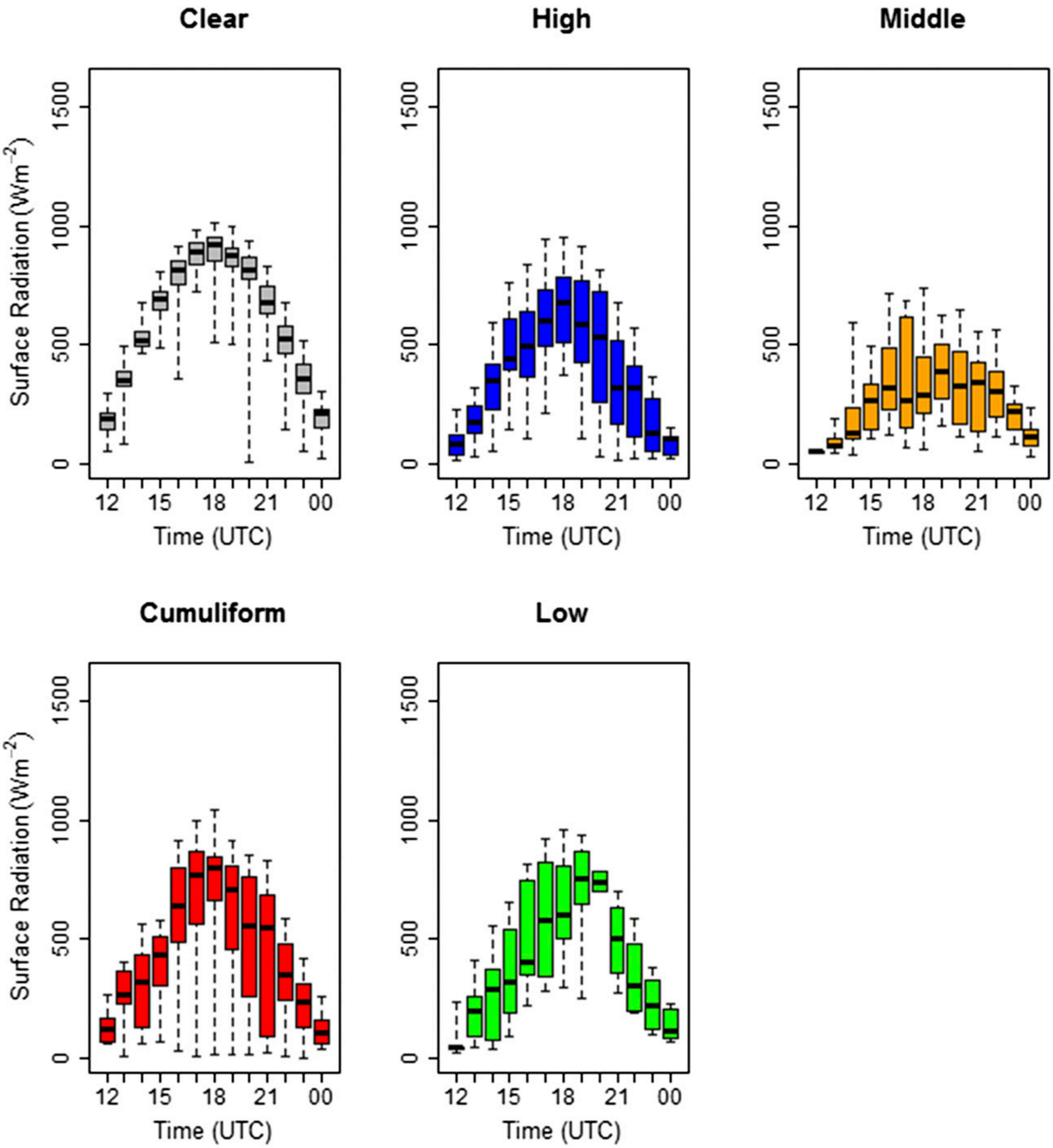

FIG. 11. As in Fig. 9, but for surface radiation.

with limitations of the NRLCC algorithm for identifying multiple levels of cloud cover typically associated with afternoon deep convection. Low and middle cloud-type groups exhibit fairly large within group variation throughout the day (Fig. 11). This large variability throughout the day suggests that the spatial coverage of such cloud cover is an important future consideration as well. Distinctions are not made among scattered low/middle cloud-type groups and more uniform low/middle cloud-type groups.

The statistical analyses bring all three datasets together in an assessment of the relationships among pavement temperatures, surface radiation and cloud-type groups. Overall, for all the collocated sites throughout the two-week 1–16 June 2011 period, there is a direct relationship between surface radiation and

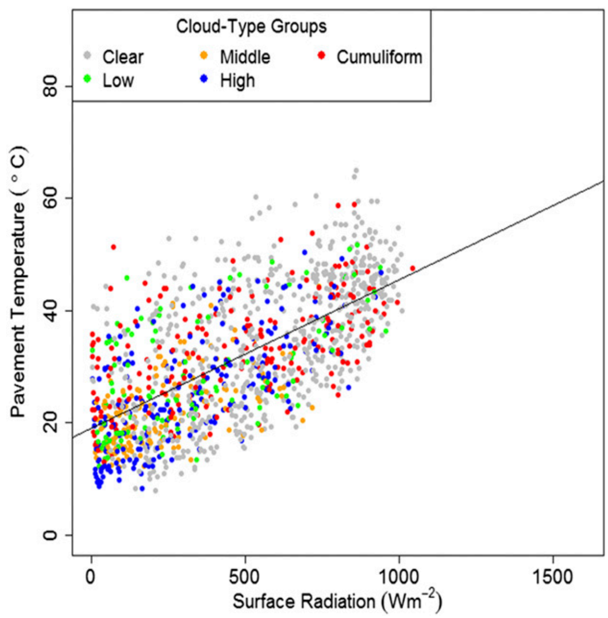

FIG. 12. Overall scatterplot of surface radiation vs pavement temperature for all 13 collocated sites for the period 1–16 Jun 2011 colored by cloud-type group. The black line is the linear regression line.

pavement temperature (Fig. 12). The correlation between surface radiation and pavement temperature is moderately strong with a correlation coefficient of 0.67 and statistically significant as well. This result means that high radiation values are associated with higher pavement temperatures. This is to be expected as both variables are also diurnally dependent, and TOD has yet to be considered. Further, this result indicates that approximately 45% of the variability in pavement temperature for this particular dataset can be explained by the surface radiation.

To account for diurnal variability, the correlation analyses are also performed at the five primary TODs (Fig. 13). Aside from sunrise, all correlation coefficients were significant. At sunrise, recall we observed our period of quasi equilibrium. A tight cluster reveals not much variability among the variables (Fig. 13). Two of the variables are weakly correlated at this period in which radiation versus pavement temperature has a nonsignificant correlation coefficient of −0.07. As the sun rises during the morning, there is more apparent separation between clear conditions and cloudy conditions when considering the scatterplot (Fig. 13). The correlation between surface radiation and pavement temperature is moderately strong during the morning TOD with a pavement temperature versus radiation coefficient of 0.72. At the midday TOD, the separation continues with clear conditions as the higher pavement temperatures coincide with the highest radiation observations. Cumuliform and high cloud-type groups are intermingled with some clear observations but are generally associated with slightly lower temperatures and radiation values. Low and middle cloud-type groups are associated with the lowest pavement temperature and surface radiation observations (Fig. 13). At this TOD, the correlation between surface radiation and pavement temperature is strongest with a coefficient of 0.83. This result suggests that during the middle of the day during the peak solar heating, despite the lag in pavement temperature, higher temperature and higher radiation are associated. Further, in the middle of the day surface radiation explains nearly 69% of the variability in pavement temperature. During the afternoon, the divisions among cloud-type group begin to decay (Fig. 13). Correlation between radiation and pavement temperature remains strong with a coefficient of 0.71. As was shown in the TOD and hourly distribution analyses, clear conditions warmed and cooled the fastest, whereas cloud conditions lagged behind in their increases and decreases. The more vertical orientation of points (i.e., steeper slope) at sunset is related to the lag of pavement temperature with the loss of solar heating and the closer association between shortwave radiation and sunlight (Fig. 13). Further, the correlation coefficient between surface radiation and pavement temperature decreases at sunset to 0.41.

Given that cloud-type groups are categorical data, a difference of medians statistical analysis for both pavement temperatures and surface radiation observations was performed at each TOD. All of the differences in medians observed at each TOD for both pavement temperature and surface radiation are significant (p value < 0.01). This boosts confidence in the aforementioned comparisons and correlations from a statistical framework.

A linear regression analysis statistically confirms the relationships observed among pavement temperatures and surface radiation during 1–16 June 2011 for the 13 collocated sites (Figs. 12 and 13). It is important to remember that the regression parameters can only be considered valid for this particular dataset. Overall, pavement temperatures vary by $0.026°\mathrm{C}\,(\mathrm{W\,m^{-2}})^{-1}$. Near sunrise (1200 UTC), the linear regression analysis confirms the quasi equilibrium with an estimated slope parameter of $-0.004°\mathrm{C}\,(\mathrm{W\,m^{-2}})^{-1}$. There is little change among pavement temperature and surface radiation early in the day because there is little direct sunlight at this TOD (Fig. 13). Later in the morning at 1500 UTC, the slope parameter increases to $0.023°\mathrm{C}\,(\mathrm{W\,m^{-2}})^{-1}$. Slope parameter estimates around midday (1800 UTC) and afternoon (2100 UTC) are identical at $0.032°\mathrm{C}\,(\mathrm{W\,m^{-2}})^{-1}$.

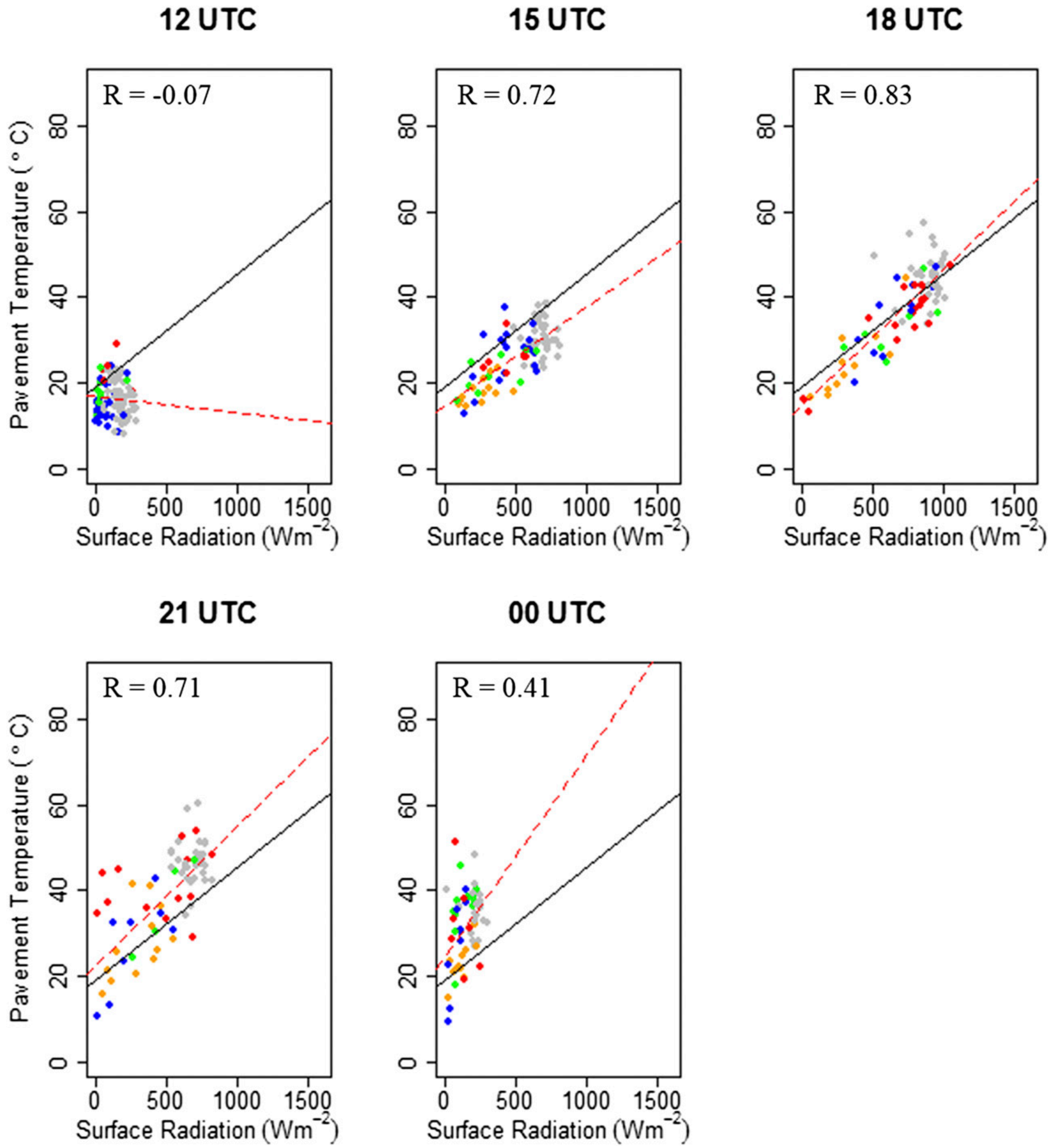

FIG. 13. TOD scatterplots of surface radiation vs pavement temperature for all 13 collocated sites for the period 1–16 Jun 2011 colored by cloud-type groups: low (green), middle (orange), high (blue), cumuliform (red), and clear (gray). The black line is the overall linear regression line shown in Fig. 12. The dashed red line represents the linear regression line for each TOD. Pearson's correlation coefficients (R) are included for each TOD in the top-left corner.

This result corresponds directly to the period of peak solar heating and typical peak surface temperatures as well. Toward sunset (0000 UTC), the linear regression estimated slope parameter increases slightly to $0.047°C (W\,m^{-2})^{-1}$. This increase in the slope is evidence of the lag associated with pavement temperatures and the reduction of direct sunlight (Fig. 13). At sunset, surface radiation drops off considerably, although pavement temperatures lag behind because of the specific heat content of the material in question (i.e., asphalt vs concrete). These statistical results quantify the role of cloud cover in influencing pavement temperatures and surface radiation and show the relationships among the variables as well.

4. Summary and conclusions

This assessment provides a first look at the application of remotely sensed cloud information to determine the influence of cloud-type groups on pavement temperature and surface radiation and the correlations among pavement temperature, surface radiation, and cloud-type groups. Results from an initial sensitivity study provide a framework for subsequent analyses. Results from a monthlong and two-week period throughout the Great Plains quantify the magnitude of influence of cloud-type groups on pavement temperature variability. Statistical analyses extend such comparisons to include surface radiation as well. There is still uncertainty as to how well the NRLCC algorithm can detect challenging (i.e., multiple level) cloud situations, though the algorithm generally performs well when considering identification output with visible satellite imagery.

This research fills a void in the literature by directly relating cloud cover to pavement temperatures. In a consideration of statistically significant differences among median pavement temperatures for the month of June 2011, clear conditions observe a median of 40.9°C. The next highest observation is with cumuliform clouds at 34.9°C. Low clouds lie in the middle of median temperatures at 31.5°C. The second-lowest cloud-type group is high clouds, with a median of 27.9°C, and the coolest group is middle clouds at 23.7°C. The results were similar for 1–16 June 2011 data as well. Considering observations at individual time stamps instead of throughout the entire dataset removes diurnal dependence and allows for more meaningful comparisons. Clear conditions are clearly associated with the highest pavement temperatures and have the smallest within-group variation throughout the day; however, they have the largest diurnal variability. Low, high, and cumuliform cloud-type groups exhibit tendencies in their pavement temperature median time series and distributions. This suggests that there is either some possible error in the NRLCC algorithm and/or optically thin high clouds will exhibit similar influence on pavement temperatures as spatially scattered (low and cumuliform) albeit optically thicker cloud-type groups. Middle clouds observed the most damped pavement temperature median time series, which is expected given the likely spatially uniform and optically thicker nature of this cloud-type group.

Pavement temperature distribution analyses among cloud-type groups and surface radiation observations reveal similar tendencies as well. This is expected as pavement temperature and surface radiation are moderately correlated (correlation coefficient of 0.67). This correlation increases to a coefficient of 0.83 when diurnal dependence is removed by considering specific TODs. Further, there is high confidence in the output from the NRLCC algorithm with the caveat that multilevel cloud situations and some low cumuliform clouds may have classification errors. Regardless, understanding these relationships is fundamental to the future goal of pavement temperature forecast improvement.

The primary research objective is achieved through the quantification of pavement temperature and cloud-type group distribution analyses. The case study analyses allow for better understanding of how cloud cover affects pavement temperature through influencing surface radiation. Satellite cross validation shows good agreement between the algorithm output and spatial association techniques with caveats noted. Ongoing research seeks to continue quantifying and considering different arrangements of cloud-type groups (e.g., spatial coverage in lieu of height groups) and the influence of such groups on pavement temperatures and surface radiation. Ultimately, the influence of cloud cover on nighttime pavement temperatures and longwave radiation must be a future avenue of research. These future studies will also have to incorporate different seasons of year as well. Understanding and quantifying these relationships is paramount to the development and feasibility assessments of assimilating cloud-type output and modeling such sensitivity with the goal of increasing the accuracy of pavement temperature forecasts.

The potential benefit of these methods could yield improved cloud data assimilation not simply for pavement temperature forecasts but for a plethora of other applications as well, such as numerical weather prediction and renewable energy forecasting. The solar energy industry, for example, could benefit from increased knowledge beyond simple observation of approaching cloud cover to more specific information of the type of cloud approaching and how that may impact photovoltaic output. These methods provide a unique observational case study approach that can be replicated as needed for various regions and across different time periods. Despite the potential benefit, it is important to caution that limitations of the methods that must be addressed include the highly variable nature of the data. Sensor and data fidelity issues in addition to site-specific information (e.g., road material, sky view and shading factors) require excellent metadata. Precipitation, longwave radiation, and multiple cloud layers further complicate the use of these satellite-based methods on relatively small spatiotemporal scales; however, the aforementioned analysis holds great promise for future consideration of improved forecasting applications. Further, with new emergent technologies these methods will likely prove invaluable to those technologies and benefit from those same technologies.

Acknowledgments. This material is based upon work supported by the American Meteorological Society Graduate Fellowship (2012-2013) sponsored by ITT Exelis and by the National Science Foundation Graduate Research Fellowship under Grant DGE-1041000. Any opinion, findings, and conclusions or recommendations expressed in this material are those of the authors and do not necessarily reflect the views of the National Science Foundation. Further, we thank collaborators at the NCAR–Research Applications Laboratory (RAL) Weather Systems and Assessment Program (WSAP) and the Significant Opportunities in Atmospheric Research and Science (SOARS) Program.

REFERENCES

Ackerman, S. A., R. E. Holz, R. Frey, E. W. Eloranta, B. C. Maddux, and M. McGill, 2008: Cloud detection with MODIS. Part II: Validation. *J. Atmos. Oceanic Technol.*, **25**, 1073–1086, doi:10.1175/2007JTECHA1053.1.

Bankert, R. L., 1994: Cloud classification of AVHRR imagery in maritime regions using a probabilistic neural network. *J. Appl. Meteor.*, **33**, 909–918, doi:10.1175/1520-0450(1994)033<0909:CCOAII>2.0.CO;2.

——, and R. H. Wade, 2007: Optimization of an instance-based GOES cloud classification algorithm. *J. Appl. Meteor. Climatol.*, **46**, 36–49, doi:10.1175/JAM2451.1.

——, C. Mitrescu, S. D. Miller, and R. H. Wade, 2009: Comparison of GOES cloud classification algorithms employing explicit and implicit physics. *J. Appl. Meteor. Climatol.*, **48**, 1411–1421, doi:10.1175/2009JAMC2103.1.

Bogren, J., 1991: Screening effects on road surface temperature and road slipperiness. *Theor. Appl. Climatol.*, **43**, 91–99, doi:10.1007/BF00865043.

Changnon, S. A., P. J. Lamb, and K. G. Hubbard, 1990: Regional climate centers: New institutions for climate services and climate-impact research. *Bull. Amer. Meteor. Soc.*, **71**, 527–537, doi:10.1175/1520-0477(1990)071<0527:RCCNIF>2.0.CO;2.

Chen, S. R., C. S. Cai, and B. Wolshon, 2009: From normal operation to evacuation: Single-vehicle safety under adverse weather, topographic, and operational conditions. *Nat. Hazards Rev.*, **10**, 68–76, doi:10.1061/(ASCE)1527-6988(2009)10:2(68).

Chen, T., W. B. Rossow, and Y. Zhang, 2000: Radiative effects of cloud-type variations. *J. Climate*, **13**, 264–286, doi:10.1175/1520-0442(2000)013<0264:REOCTV>2.0.CO;2.

CLASS, 2014: Environmental data from geostationary satellites. NOAA, accessed 2 December 2014. [Available online at http://www.nsof.class.noaa.gov/saa/products/search?datatype_family=GVAR_IMG.]

Crevier, L., and Y. Delage, 2001: METRo: A new model for road-condition forecasting in Canada. *J. Appl. Meteor.*, **40**, 2026–2037, doi:10.1175/1520-0450(2001)040<2026:MANMFR>2.0.CO;2.

Drobot, S., M. Chapman, C. Burghardt, S. Linden, and J. Cowie, 2012: The Toyota Racing Development Pavement Forecast Project. NCAR, 90 pp.

Federal Highway Administration, 2014: Road Weather Management Program. [Available online at http://ops.fhwa.dot.gov/weather/q1_roadimpact.htm.]

Hallowell, R. G., and G. L. Blaisdell, 2003: Automated forecasting of road conditions and recommended road treatments for winter storms. Preprints, *19th Conf. on Interactive Information and Processing Systems*, Long Beach, CA, Amer. Meteor. Soc., 10.6. [Available online at https://ams.confex.com/ams/pdfpapers/55538.pdf.]

Hartmann, D. L., M. E. Ockert-Bell, and M. L. Michelsen, 1992: The effect of cloud type on Earth's energy balance: Global analysis. *J. Climate*, **5**, 1281–1304, doi:10.1175/1520-0442(1992)005<1281:TEOCTO>2.0.CO;2.

High Plains Regional Climate Center, 2013: Climate data services classic online services. Accessed 1 June 2013. [Available online at http://www.hprcc.unl.edu/onlinedataservices.php.]

Khasawneh, M. A., and R. Y. Liang, 2012: Temperature effect on frictional properties of HMA at different polishing sites. *Jordan J. Civ. Eng.*, **6**, 39–53.

Liu, L., X. Sun, F. Chen, S. Zhao, and T. Gao, 2011: Cloud classification based on structure features of infrared images. *J. Atmos. Oceanic Technol.*, **28**, 410–417, doi:10.1175/2010JTECHA1385.1.

MADIS, 2014: Meteorological Assimilation Data Ingest System. Accessed 1 June 2013. [Available online at http://madis.noaa.gov/.]

NCAR, 2007: A comparison of road temperature models: FASST, METRo, and SNTHERM. Version 2.0, 24 pp. [Available online at https://www.rap.ucar.edu/projects/rdwx_mdss/documents/RoadModel_Comparison_Report_v2.0_8_3_07.pdf.]

——, 2011: Maintenance Decision Support System. Federal Highway Administration Office of Transportation Operations. [Available online at http://ral.ucar.edu/projects/rdwx_mdss/.]

——, 2014: High Performance Storage System. [Available online at https://www2.cisl.ucar.edu/docs/hpss.]

NOAA, 2014: Weather-Ready Nation. [Available online at http://www.nws.noaa.gov/com/weatherreadynation/.]

NRL, 2013: NRL Monterey GOES cloud classification. [Available online at http://www.nrlmry.navy.mil/sat-bin/clouds.cgi.]

Pisano, P. A., L. C. Goodwin, and M. A. Rosetti, 2008: U.S. highway crashes in adverse road weather conditions. *24th Conf. on Interactive Information and Processing Systems*, New Orleans, LA, Amer. Meteor. Soc., 8.1. [Available online at https://ams.confex.com/ams/pdfpapers/133554.pdf.]

Ricchiazzi, P., S. Yang, C. Gautier, and D. Sowle, 1998: SBDART: A research and teaching software tool for plane-parallel radiative transfer in the earth's atmosphere. *Bull. Amer. Meteor. Soc.*, **79**, 2101–2114, doi:10.1175/1520-0477(1998)079<2101:SARATS>2.0.CO;2.

Rutz, J. J., and C. V. Gibson, 2013: Integration of a road surface model into NWS operations. *Bull. Amer. Meteor. Soc.*, **94**, 1495–1500, doi:10.1175/BAMS-D-12-00037.1.

SBDART, 2013: SBDART: A practical tool for plane-parallel radiative transfer in Earth's atmosphere. Accessed 11 November 2013. [Available online at http://paulschou.com/tools/sbdart.]

Stephens, G. L., 2005: Cloud feedbacks in the climate system: A critical review. *J. Climate*, **18**, 237–273, doi:10.1175/JCLI-3243.1.

——, and S. C. Tsay, 1990: On the cloud absorption anomaly. *Quart. J. Roy. Meteor. Soc.*, **116**, 671–704, doi:10.1002/qj.49711649308.

Tag, P. M., R. L. Bankert, and L. R. Brody, 2000: An AVHRR multiple cloud-type classification package. *J. Appl. Meteor.*, **39**, 125–134, doi:10.1175/1520-0450(2000)039<0125:AAMCTC>2.0.CO;2.

Várnai, T., and R. Davies, 1999: Effects of cloud heterogeneities on shortwave radiation: Comparison of cloud-top variability and internal heterogeneity. *J. Atmos. Sci.*, **56**, 4206–4224, doi:10.1175/1520-0469(1999)056<4206:EOCHOS>2.0.CO;2.

Yang, J., W. Lu, Y. Ma, and W. Yao, 2012: An automated cirrus cloud detection method for a ground-based cloud image. *J. Atmos. Oceanic Technol.*, **29**, 527–537, doi:10.1175/JTECH-D-11-00002.1.